eprints@whiterose.ac.uk
https://eprints.whiterose.ac.uk/

The White Dwarf Binary Pathways Survey I: A sample of FGK stars with white dwarf companions

S. G. Parsons[1]★, A. Rebassa-Mansergas[2], M. R. Schreiber[1,3], B. T. Gänsicke[4], M. Zorotovic[1] and J. J. Ren[5]

[1] *Instituto de Física y Astronomía, Universidad de Valparaíso, Avenida Gran Bretana 1111, Valparaíso, 2360102, Chile*
[2] *Departament de Física, Universitat Politécnica de Catalunya, c/Esteve Terrades 5, 08860 Castelldefels, Spain*
[3] *Millenium Nucleus "Protoplanetary Disks in ALMA Early Science", Universidad de Valparaiso, Valparaiso 2360102, Chile*
[4] *Department of Physics, University of Warwick, Coventry CV4 7AL, UK*
[9] *Department of Astronomy, Peking University, Beijing 100871, P. R. China*

ABSTRACT

The number of spatially unresolved white dwarf plus main-sequence star binaries has increased rapidly in the last decade, jumping from only ∼30 in 2003 to over 3000. However, in the majority of known systems the companion to the white dwarf is a low mass M dwarf, since these are relatively easy to identify from optical colours and spectra. White dwarfs with more massive FGK type companions have remained elusive due to the large difference in optical brightness between the two stars. In this paper we identify 934 main-sequence FGK stars from the Radial Velocity Experiment (RAVE) survey in the southern hemisphere and the Large Sky Area Multi-Object Fiber Spectroscopic Telescope (LAMOST) survey in the northern hemisphere, that show excess flux at ultraviolet wavelengths which we interpret as the likely presence of a white dwarf companion. We obtained Hubble Space Telescope ultraviolet spectra for nine systems which confirmed that the excess is indeed caused, in all cases, by a hot compact companion, eight being white dwarfs and one a hot subdwarf or pre-helium white dwarf, demonstrating that this sample is very clean. We also address the potential of this sample to test binary evolution models and type Ia supernovae formation channels.

Key words: binaries: close – stars: white dwarfs – stars: early-type – stars: evolution

1 INTRODUCTION

Around 25 per cent of all binary stars are born close enough that they will eventually interact with each other when the more massive member of the binary evolves off the main-sequence and becomes a giant star (Willems & Kolb 2004). Very often this results in material flowing from the expanding giant onto the lower mass star, which cannot incorporate it fast enough and therefore the material overflows the lower-mass star's Roche lobe, leading to the entire binary being engulfed in what is known as a common envelope (CE, Paczynski 1976; Webbink 1984). Inside this envelope the stars are subject to strong frictional forces leading to a loss of angular momentum and orbital energy, hence the two stars spiral inward towards each other, ejecting the envelope as they do so. What emerges from the CE is a close binary, known as a post common-envelope binary (PCEB), containing the core of the giant star (which will become a white

dwarf) and its main-sequence star companion. Depending upon the stellar masses and final separation after the CE stage, the binary may go on to experience a second CE stage when the main-sequence star evolves, resulting in a double degenerate binary system (Webbink 1984; Nelemans et al. 2001; Toonen et al. 2012). Alternatively, the stars may have emerged from the CE close enough to each other that angular momentum loss will drive them in to contact before the main-sequence star has evolved, often leading to the formation of a cataclysmic variable (CV) system.

PCEBs are important objects since they are likely the progenitors of supernova Ia (SN Ia). While it is generally established that SN Ia are the result of the thermonuclear ignition of a carbon-oxygen core white dwarf, there is not yet a consensus on the pathway leading to the explosion. In the classic double degenerate scenario the merger of two white dwarfs with a combined mass above the Chandrasekhar limit leads to a SN Ia explosion (Tutukov & Yungelson 1979; Webbink 1984). This channel has the advantage that it can produce systems with both long and short time delays

★ steven.parsons@uv.cl

and explain the lack of hydrogen and helium lines in most SN Ia spectra (Branch et al. 1995). Moreover, there is both theoretical and observational evidence for a large population of close double white dwarf binaries (Yungelson et al. 1994; Nelemans & Tout 2005; Napiwotzki et al. 2001). However, there is some uncertainty as to whether the merger leads to an explosion or rather a core collapse and the formation of a neutron star instead (Nomoto & Kondo 1991) and at present the situation remains uncertain (Yoon et al. 2007). Moreover, a range of explosion masses are possible with the merger of two white dwarfs of arbitrarily mass, which would cause a spread in the luminosities of SN Ia, affecting their use as standard candles. In the alternative scenario, known as the single degenerate channel, a white dwarf stably accretes material from a nondegenerate companion star until it grows to the Chandrasekhar mass and explodes (Iben & Tutukov 1984). In this case the progenitor systems are thought to be white dwarfs accreting from main-sequence or giant stars at a sufficiently high rate that hydrogen is stably burnt on the surface of the white dwarf, avoiding nova explosions (Shara et al. 1977; Iben 1982). Such systems are observed in the Galaxy and Magellanic Clouds (van den Heuvel et al. 1992; Kahabka & van den Heuvel 1997) and are known as supersoft X-ray sources (SSSs). However, in order to sufficiently grow the white dwarf, models often require fine-tuning many uncertain input parameters such as the accretion rate (Hillebrandt & Niemeyer 2000; Wang & Han 2012). Furthermore, the single degenerate channel has difficulty in creating SN Ia with time delays larger than a few Gyr due to the short main-sequence lifetimes of their progenitors (e.g. Claeys et al. 2014).

In recent years the idea of sub-Chandrasekhar or double-detonation models have become popular. In this model the white dwarf has accumulated a substantial surface layer of helium. When this layer ignites it can send a strong shock wave into the core of the white dwarf, compressing it and triggering a secondary detonation of the core, leading to a SN Ia explosion (Fink et al. 2007; Sim et al. 2010; Kromer et al. 2010). This can be achieved via the double degenerate route, with the merger of a carbon-oxygen core and a helium core white dwarf, or the single degenerate route, with the white dwarf accreting material from a helium-rich companion star. This idea has the advantage that there are a sufficient number of such binaries to explain the birthrate of SN Ia (Ruiter et al. 2009), although it is difficult to explain the observed similarities in most SN Ia via this model (e.g. Branch et al. 1995). In virtually every model for the formation of SN Ia the progenitor systems are binaries that have passed through at least one CE event (two in the case of the double degenerate channel), hence PCEBs are a valuable population for testing the ideas of SN Ia formation. In particular, PCEBs containing white dwarfs with massive FGK-type main-sequence star companions are both potential SN Ia progenitors (via the single degenerate channel) and an intermediate stage (via the double degenerate channel) and therefore are a particularly useful population. A large sample of such systems can even be used to estimate the relative number of systems evolving through the double degenerate and the single degenerate channels.

The number of PCEBs with late-type companions has rapidly increased in the last few years thanks mainly to the Sloan Digital Sky Survey (SDSS) and its spectroscopic database (Raymond et al. 2003; Silvestri et al. 2006; Rebassa-Mansergas et al. 2007, 2012a; Li et al. 2014). With optical spectra alone it is possible to detect even very cool white dwarfs next to M-type stars (e.g. Parsons et al. 2012) and hotter white dwarfs are still detectable with companions up to very-late K (∼5 per cent of SDSS white dwarf plus main-sequence star binaries contain K star components, Rebassa-Mansergas et al. 2016). However, detecting PCEBs with earlier-type companions is more chalenging because these hotter, larger main-sequence stars completely outshine white dwarfs in the optical, implying that a combination of ultraviolet (UV) and optical data is required.

Several attempts have been made to identify white dwarfs with FGK-type main-sequence star companions (e.g. Maxted et al. 2009), which have succeeded in finding these systems, but have failed to produce large numbers of them. For example, SDSS FGK stars are generally located at large enough distances that all but the very hottest white dwarfs will go undetected in UV surveys, severely reducing the sample size. Previous studies of the far-UV and soft X-ray spectra of main-sequence stars have revealed the presence of white dwarf companions (Landsman et al. 1993; Barstow et al. 1994; Vennes et al. 1995; Christian et al. 1996; Landsman et al. 1996; Vennes et al. 1997; Burleigh et al. 1997; Burleigh & Barstow 1998; Burleigh et al. 1998; Burleigh & Barstow 1999), but the vast majority of these systems are visually resolved binaries that were formed far enough apart that they avoided a CE event. To date, only 7 PCEBs with early-type main-sequence star companions have been identified and had their orbital periods measured (Nelson & Young 1970; Simon et al. 1985; Berghöfer et al. 2000; Vennes et al. 1998; Kruse & Agol 2014; Parsons et al. 2015). The difficulty in detecting white dwarf companions to FGK stars is not only due to the extreme optical contrast between the two stars (typically the white dwarf will only contribute ∼1 per cent of the potical light), but also due to the fact that many of the largest samples of FGK stars (e.g. from the SDSS) are lacking in bright (V<12) members because they saturate in modern survey data. This means that these samples contain fainter stars that are located at large distances. For example, the saturation limits for SDSS (about 14 mag in g, r and i and about 12 mag in u and z, Chonis & Gaskell 2008) mean that main-sequence FGK stars are generally located at more than 0.5 kpc from Earth (Bilir et al. 2009). At these large distances only the hottest (hence youngest and most short-lived) white dwarf companions will be bright enough to be detected in the UV, severely limiting the sample size (only ∼2 per cent of UV-excess FGK stars in SDSS are the result of a white dwarf companion, Smith et al. 2014). Therefore, searching for PCEBs with early-type companions requires a sample of bright, nearby FGK stars with UV data.

To this end, we have started a project that uses data from surveys that target bright FGK stars in combination with UV data from the Galaxy Evolution Explorer (GALEX) database in order to detect main-sequence stars with substantial UV-excess colours that we interpret as the result of a nearby white dwarf companion. Follow-up ground-based spectroscopic observations can then be used to distinguish between the close PCEBs and wide systems that

avoided a CE event. The final aim of this project is to establish the first large sample of PCEBs with early-type components, suitable for population synthesis studies and useful for testing models of SN Ia formation. The first result from this project Parsons et al. (2015) was the identification of TYC 6760-497-1 as a white dwarf plus F-star in a 12 hour binary, which is the first known progenitor of a SSS, i.e. the white dwarf will grow in mass in its future evolution. In this paper we present the initial step in our project, the selection process and sample of UV-excess FGK stars. The spectroscopic follow-up data and identification of PCEB/wide systems will be presented in a future paper. We have also obtained Hubble Space Telescope (*HST*) UV spectroscopy of 9 of these stars that unambiguously prove that the excesses are indeed due to white dwarfs and we present these data in this paper.

2 SAMPLE SELECTION

In this section we outline the methods we used to select our sample of FGK main-sequence stars with UV-excesses. Note that these stars may be close, short-period PCEBs (the main targets of this project), or they may be wide[1] white dwarf plus FGK binaries, or they may be a chance alignment of an FGK star with a foreground or background white dwarf. Other potential sources of contamination are discussed in Section 5.1.

We used data from two surveys, the Radial Velocity Experiment (RAVE) survey in the southern hemisphere and the Large Sky Area Multi-Object Fiber Spectroscopic Telescope (LAMOST) survey in the northern hemisphere. We begin by discussing these two samples separately.

2.1 The southern hemisphere sample

In order to identify main-sequence FGK stars with UV-excesses in the southern hemisphere sky, we used data from the RAVE survey[2] data release 4 (Kordopatis et al. 2013). RAVE is a magnitude limited survey of randomly selected southern hemisphere stars spanning $9< I <12$. It has collected spectra for over 425,000 stars covering the infrared calcium triplet $(8410-8795\text{Å})$ with a resolution of $R \sim 7500$ using the 6dF facility on the 1.2m Schmidt Telescope at Anglo-Australian Observatory in Siding Spring, Australia. The data are then used to determine atmospheric parameters (effective temperature, surface gravity, metallicity) as well as a measurement of the radial velocity of the star. For a more detailed description of the RAVE survey we refer the reader to Kordopatis et al. (2013) and references therein.

We selected all the main-sequence (non-giant, $\log g >$ 3.5) stars in the RAVE survey with effective temperatures between 4,000 K and 7,000 K (corresponding to F, G and K stars) and cross correlated them with UV data from the GALEX survey (Martin et al. 2005), selecting all the sources

---

[1] Throughout this paper, the term *wide binaries* refers to systems that did not undergo CE evolution. Such systems may have orbital separations of as little as ~10 AU, and can therefore remain unresolved in the available imaging, hence we note that *wide* should not be mistaken for *spatially resolved*.
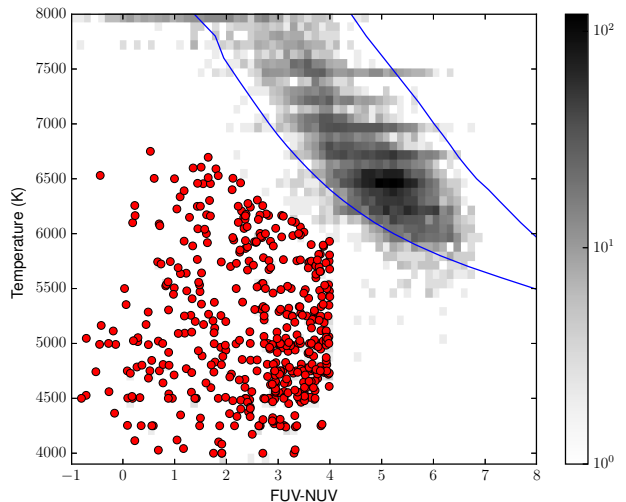[2] https://www.rave-survey.org

Figure 1. Distribution of the 23,484 RAVE dwarf stars ($\log g >$ 3.5) with both a GALEX FUV and NUV detection. The temperatures are taken directly from the RAVE DR4 catalogue. Shown in blue are two theoretical tracks computed from PHOENIX atmospheric models, one with a high metallicity and high surface gravity ($\log Z = +1$ $\log g = 5.0$, top curve) and one with a low metallicity and low surface gravity ($\log Z = -3$ $\log g = 3.5$, bottom curve). These represent extreme limits on the colours of main-sequence stars. The vast majority of RAVE stars fall within these extreme models, as expected. The red points mark the 430 targets that fall within our cut (FUV−NUV<4, T>4000 K and FUV−NUV at least 1.5 magnitudes bluer than the bottom model).

with both far-UV (FUV) and near-UV(NUV) measurements (with errors below 0.2 mag and no artifacts associated to their photometry), resulting in 23,484 main-sequence stars with good UV photometry. The distribution of effective temperatures and FUV−NUV colours of these stars are shown in Figure 1.

We used the extensive library of PHOENIX stellar synthetic spectra from Husser et al. (2013) to determine the UV colours of single main-sequence stars over a range of temperatures by convolving the synthetic spectra with the GALEX FUV and NUV filter profiles. We used synthetic spectra spanning surface gravities of $3.5< \log g <5.0$ and metallicities of $-3.0< \log Z <1.0$, but did not include any alpha element enhancement or depletion. We found that the UV colours of main-sequence stars are strongly affected by both their surface gravity (due to the surface gravity dependence in the strength of the Balmer jump, and the associated suppression of NUV flux) and their metallicity (which causes variations in the UV opacity), leading to a spread in the FUV−NUV colour of almost 3 magnitudes for stars with the same effective temperature[3]. In Figure 1 we plot two tracks showing the UV colours of the bluest and reddest main-sequence stars within our parameter range. We expect single FGK main-sequence star from RAVE to have UV colours somewhere between these two tracks. Indeed, Figure 1 shows that the FUV−NUV colours of the vast majority of FGK stars in RAVE fall within these two extremes ($\simeq 99$ per cent). How-

---

[3] activity is likely to further increase the intrinsic scatter, particularly for the lower mass stars
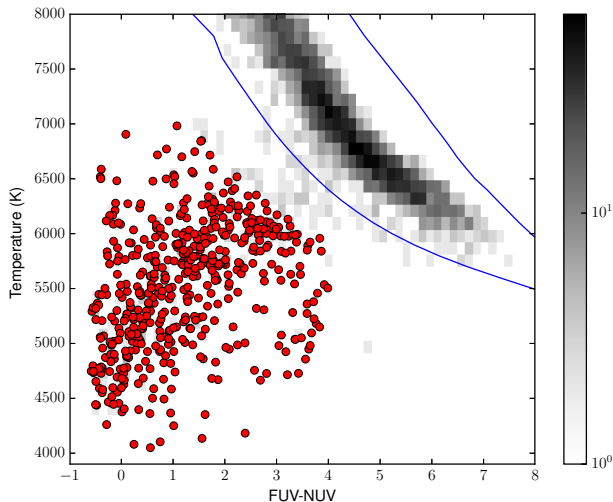
Figure 2. The UV colours and temperatures of LAMOST main-sequence FGK stars. We plot the same two PHOENIX models shown in Figure 1, which represent the most extreme colours for main-sequence stars. Stars flagged as having UV-excesses are shown as red points and have UV colours at least 1.5 magnitudes bluer than the bottom model. The LAMOST sample does not suffer from the same discretisation issue seen in the RAVE sample, hence why it appers smoother.

ever, there are also a small number of stars with substantially bluer UV colours which may be caused by the presence of a nearby white dwarf companion. We flag a star as having a UV-excess if it has a FUV−NUV colour at least 1.5 magnitudes bluer than the bluest main-sequence star models for its effective temperature(the bottom curve in Figure 1). We also place an upper limit on the FUV−NUV colour of 4, to avoid including any stars with erroneous RAVE temperatures.

In total our sample contains 430 stars with UV-excesses, these are highlighted in Figure 1 as red points and are detailed in Table A1 in the appendix. The completeness and any sources of bias in our sample will be addressed in a future paper.

We checked our sample of UV-excess FGK stars against the list of white dwarf's with early-type companions from Holberg et al. (2016). We found that only 4 of the 98 objects from the Holberg et al. (2016) catalogue are in the RAVE survey, and only one of these, WD 0354-368 (53,000K white dwarf plus G2 star with a sky projected separation of ∼0.5″), has GALEX FUV and NUV measurements (most objects in the Holberg et al. (2016) catalogue are too bright for GALEX). However, this star did make it into our cut.

2.2 The northern hemisphere sample

The Large sky Area Multi-Object fiber Spectroscopic Telescope (LAMOST) is a ≃4 meter effective aperture Meridian reflecting Schmidt telescope with a 5 degrees diameter field of view (Cui et al. 2012; Luo et al. 2012; Yuan et al. 2015). As a dedicated-survey telescope, LAMOST makes use of spectral plates to observe 4,000 spectroscopic plus calibration targets in one single exposure, equally distributed among 16 fiber-fed spectrographs. The spectra cover the en-
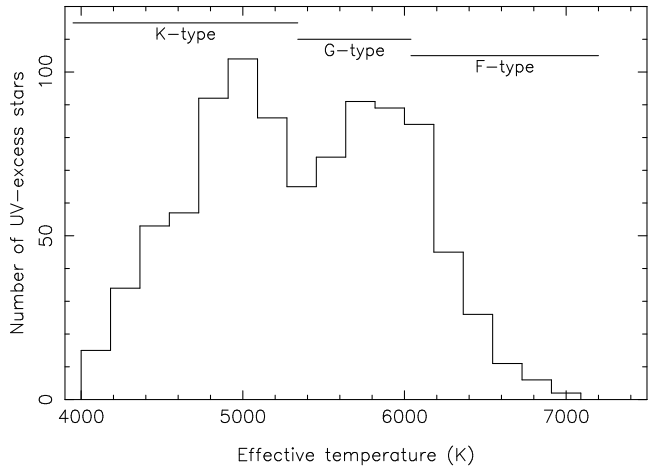

Figure 3. The distribution of temperatures of the UV-excess stars in our combined RAVE+LAMOST sample. The approximate temperature ranges for standard ($\log g$ = 5) F, G and K type main-sequence stars are indicated at the top of the plot.

tire optical wavelength range (≃3,700−9,000Å) at a resolving power of ∼2,000. The two main surveys carried out by LAMOST are LEGAS (the LAMOST Extra-Galactic Survey of galaxies), that aims at studying the large scale structure of the Universe (Zhao et al. 2012), and LEGUE (the LAMOST Experiment for Galactic Understanding and Exploration), that aims at obtaining millions of main-sequence star spectra to study the structure and evolution of the Milky Way (Deng et al. 2012). Unlike the SDSS, the LEGUE survey follows a target selection algorithm that is not restricted by a lower magnitude limit (Zhao et al. 2012; Carlin et al. 2012), thus allowing collection of a large number of main-sequence star spectra that are bright enough to search for white dwarf companions. This, together with the fact that the LAMOST is located in the Xinglong observing station of China, allows us to complement our search of white dwarf plus FGK binaries in the northern hemisphere.

From 2012 September, the LAMOST has been performing a five-year regular survey. Before that there was a one-year pilot survey followed by a two-year commissioning survey. The current data product of the LAMOST that is publicly available is data release 1 (DR1). DR1 contains a total of 2,204,696 spectra, 1,944,392 of which are catalogued as main-sequence stars by the LAMOST pipeline (Luo et al. 2015). Of these, 794,371 are flagged as F, G or K main-sequence stars and all of them have effective temperature, surface gravity and metallicity values derived via the LAMOST stellar parameter pipeline (Wu et al. 2014; Xiang et al. 2015). We selected only those objects having spectra with a signal-to-noise ratio of greater than 10, to ensure that the stellar parameters are robust.

We cross-correlated the ∼800,000 LAMOST FGK main-sequence stars with GALEX and found NUV and FUV detections for 4632 objects. In all cases the ultraviolet magnitude errors were below 0.2 mag and no artifacts were associated to their photometry. As for the RAVE sample, we selected white dwarf plus FGK binary candidates based on the detection of an ultraviolet excess, defined as being, for a given temperature, 1.5 magnitudes bluer than the bluest
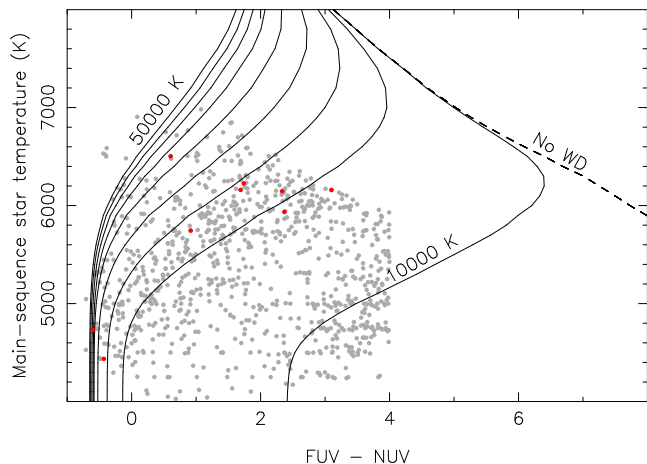
Figure 4. The effect of a white dwarf companion on the UV colours of main-sequence stars. The dashed line shows the FUV–NUV of $\log g$ = 4.5, solar metallicity main-sequence stars as computed from PHOENIX models. The solid lines show how the colours of these stars are changed due to the presence of a $\log g$ = 8.0 white dwarf companion at the same distance. The white dwarf temperatures increase in steps of 5000 K from right to left. The gray points correspond to our RAVE/LAMOST UV-excess objects and the red points are those for which we have obtained *HST* UV spectra.

Figure 5. Same as Figure 4 but placing 20,000K white dwarfs with varying surface gravity next to $\log g$ = 4.5, solar metallicity main-sequence stars. The white dwarf surface gravity increases from left to right in steps of 0.5 dex.

PHOENIX main-sequence colour track (see Figure 2). The total number of LAMOST FGK stars with UV-excesses selected in this way is 504. These objects are detailed in Table B1 in the appendix. As with the RAVE sample, there was only one previously known system from the Holberg et al. (2016) catalogue in the LAMOST database with good UV photometry, WD 1024+326 (an unresolved 41,000K white dwarf plus G5 system) and this system made it into our cut.

3 PROPERTIES OF THE SAMPLE

In total we have found 934 (430 from RAVE, 504 from LAMOST) main-sequence FGK stars that show a UV-excess that may be indicative of the presence of a nearby white dwarf companion. In Figure 3 we show the distribution of temperatures (and approximate spectral types) for these stars. Approximately half our sample consists of K-type stars (471 objects), whilst one third are G-type stars (307 objects) and the remainder are F-type stars(156 objects).

To estimate the range of white dwarf parameters that our sample can probe, we combined the PHOENIX model spectra of main-sequence stars with synthetic spectra of white dwarfs from Koester (2010). We used the Torres relation (Torres et al. 2010) to estimate the radius of the main-sequence star, and the cooling models of Holberg & Bergeron (2006) to estimate the radius of the white dwarf. We then combined the spectra of both stars and computed the resulting NUV–FUV colour. In Figure 4 we show the effects on the NUV–FUV colour of varying the temperature of the white dwarf, while keeping its surface gravity fixed at $\log g$ = 8.0. The figure shows that our sample could potentially contain systems with white dwarfs as cool as 10,000K next to K stars, 15,000K next to G stars and 20,000K next to F stars, hence covering a large range
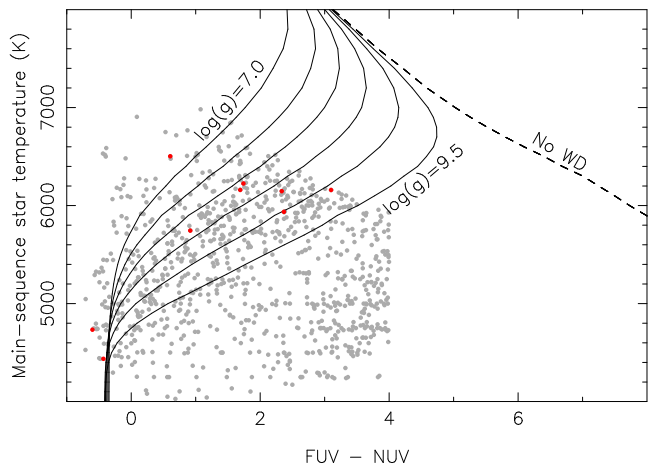
of cooling times. However, the effects of surface gravity are also important. Figure 5 shows the results of keeping the temperature of the white dwarf fixed at 20,000K and varying it's surface gravity. The figure shows that surface gravity only has a very minor effect on the detectability of a white dwarf next to a K star and only a moderate effect next to a G star. However, when placed next to an F star the surface gravity of the white dwarf is important for its detectability. High surface gravity (hence more massive and smaller) white dwarfs only contribute a small fraction of the overall UV flux against an F star and hence these binaries would not be detected in our cut. The situation is better at higher temperatures, above ~25,000K any white dwarf should be detected, regardless of its surface gravity. Therefore, our sample of systems with F stars likely contains only the younger members. Fortunately, given the shorter main-sequence lifetimes of F stars (compared to later spectral types), there is unlikely to be a large population of these stars with cool ($T_{\rm eff}$ < 20,000K) white dwarf companions.

To reinforce this point we simulated the evolution of a population of binaries with FGK-type secondary stars in order to see the distribution of white dwarf temperatures in the resulting population. The simulations were performed in the same way as in Zorotovic et al. (2014b) assuming a flat initial-mass-ratio distribution, a common envelope efficiency of 0.25, solar metallicity and without any contribution from recombination energy. Our results include all type of detached white dwarf plus FGK systems, not only PCEBs, but also wide system. The binary star evolution code from Hurley et al. (2002) uses very old models (Mestel 1952) to calculate the white dwarf effective temperature. Therefore, more accurate values were calculated following Zorotovic et al. (2016) i.e. by using the cooling tracks from Althaus & Benvenuto (1997) and from Fontaine et al. (2001) for helium-core or carbon/oxygen-core white dwarf respectively. Figure 6 clearly shows that there is a lack of systems containing white dwarfs with temperatures below ~15,000K with F-type companions (which would be found in the top-left of the plot), because the F stars have also evolved and these systems are now double white dwarf bina-
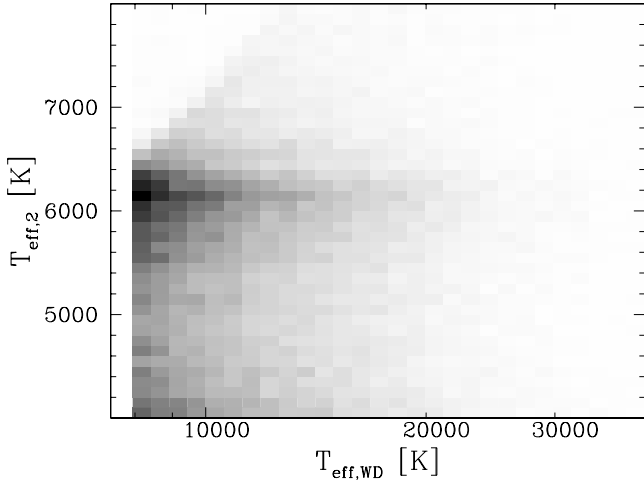
Figure 6. Simulated distribution of white dwarf and main-sequence star temperatures. Our sample of UV-excess objects does not cover systems containing cool ($T_{\rm eff}$ < 20,000K) white dwarfs and hot (F-type, $T_{\rm eff}$ >= 6,500K) main-sequence stars. However, this plot shows that the population of systems of this type is very minor and therefore we are not missing a large number of systems. The intensity of the grey-scale represents the density of simulated objects in each bin, on a linear scale, and normalized to one for the bin that contains most systems.
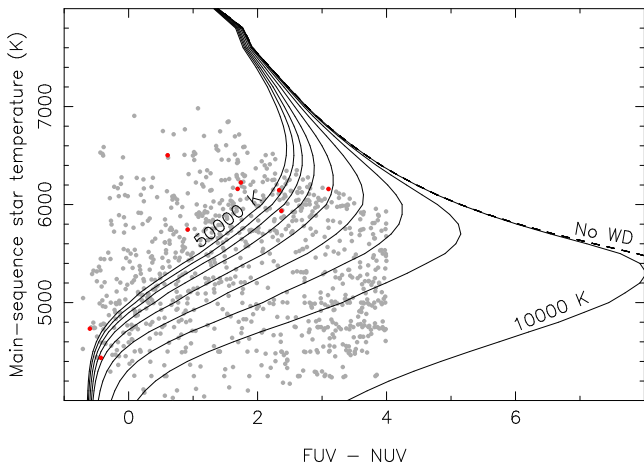

Figure 7. Same as Figure 4 but with a $\log g$ = 3.5 metal poor ($\log Z = -3.0$) main-sequence star.

ries. Figure 6 does suggest that we are missing a small number of F stars with 15,000-25,000K white dwarf companions. Note that it is possible for main-sequence stars with a large range of masses to all have temperatures close to 6,200K (stars between 1.0 and 1.5M$_\odot$ can have temperatures close to 6,200K depending upon their surface gravity) and hence there is a peak in the distribution shown in Figure 6 for stars of this temperature.

Finally, the parameters of the main-sequence star (beyond its surface temperature) also have an effect on the detectability of a white dwarf companion. In Figure 7 and Figure 8 we show the same plots as before, but with low surface gravity, metal poor main-sequence stars, which have the bluest UV colours. In this case the detectability is re-
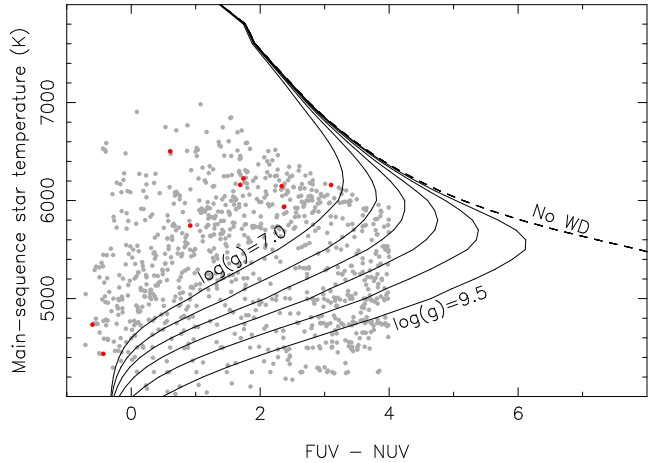

Figure 8. Same as Figure 5 but with a $\log g$ = 3.5 metal poor ($\log Z = -3.0$) main-sequence star.

duced in all circumstances and is particularly challenging in the case of F stars, where even the hottest white dwarfs only produce an excess of one magnitude, hence our sample is likely to contain only very few such stars. Only 5 per cent of our UV-excess stars are metal poor ($\log Z < -1$) and all of these are K stars. Likewise, only 25 per cent of our sample are low surface gravity stars ($\log g < 4$), of which the majority (65 per cent) are K stars and most of the rest (30 per cent) are G stars.

4   HUBBLE SPACE TELESCOPE UV OBSERVATIONS

### 4.1   Observations and their reduction

We spectroscopically observed 9 UV-excess objects with *HST* in order to confirm that the excess is due to a white dwarf companion. Depending upon the brightness of the target we either used the Space Telescope Imaging Spectrograph (STIS) or the Cosmic Origins Spectrograph (COS). All observations we obtained within program GO 13704 between October 2014 and July 2015 and are summarised in Table 1. For the STIS observations we used the G140L grating centered on 1425Å and for the COS observations we used the G130M grating centered on 1291Å. Each target was observed for one spacecraft orbit. The data were processed using CALSTIS V3.4 and CALCOS V3.1.

4.2   Results

We show the STIS and COS spectra in Figure 9 and Figure 10 respectively. We confirm the presence of a white dwarf in 8 of the 9 observed systems. The analysis of TYC 6760-497-1, which also contains a white dwarf, was previously presented in Parsons et al. (2015) and is not shown again. One system, LAMOST J1528+4305, appears to contain a pre-white dwarf object. In this case the narrow Lyα line implies that this object has a low surface gravity ($\log g \sim 5$), which is too low for a typical white dwarf. However, the blue continuum slope shows that the UV flux originates from a hot star and is clearly not from the 4,700 K main-sequence star seen
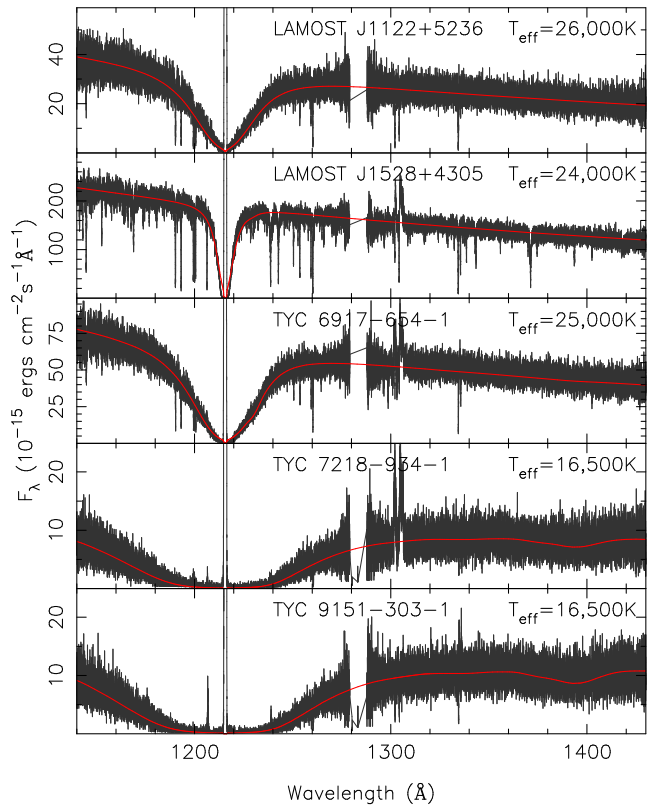
Table 1. Log of *HST* observations.

Target	Instrument	JD start	Exp (s)
CD-68 2365	STIS	2457182.2344	2712
LAMOST J1122+5236	COS	2457015.3989	2309
LAMOST J1445+1236	STIS	2457131.3753	2362
LAMOST J1528+4305	COS	2456961.7038	2109
TYC 6760-497-1	STIS	2457031.7870	2381
TYC 6917-654-1	COS	2456987.8214	1977
TYC 6996-449-1	STIS	2457001.6869	2418
TYC 7218-934-1	COS	2457151.5144	2175
TYC 7218-934-1	COS	2457150.4747	2175
TYC 9151-303-1	COS	2457233.8558	2440
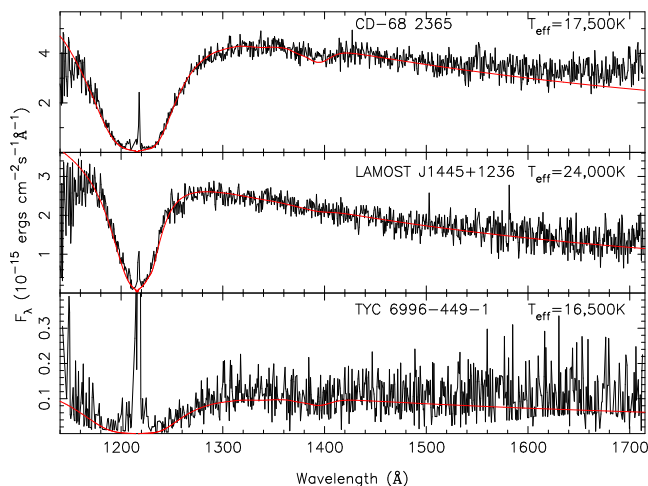
Figure 9. *HST* STIS UV spectra of three of our UV-excess objects, clearly showing that the excess is the result of a nearby white dwarf. Also shown are the best fit white dwarf model spectra assuming a mass of 0.6M$_\odot$.

Figure 10. *HST* COS UV spectra of five of our UV-excess objects, clearly showing that the excess is the result of a nearby white dwarf. Also shown are the best fit white dwarf model spectra assuming a mass of 0.6M$_\odot$, with the exception of LAMOST J1528+4305, that cannot be fitted with a standard white dwarf model (see text). A *logg* = 5 model is shown instead.

in the optical. Therefore, this hot object is fainter than the main-sequence star in the optical and hence must be smaller. Therefore, we suspect that this object could be either a hot subdwarf star or a pre-helium white dwarf (similar to the objects seen in EL CVn type binaries Maxted et al. 2014). The spectra of LAMOST J1122+523, LAMOST J1528+4305 and TYC 6917-654-1 also show narrow metal lines that may either be interstellar or due to the white dwarf accreting wind material from the main-sequence star, which may be an indication that some of these systems are close binaries (e.g. Parsons et al. 2015). All the spectra also show some geocoronal emission in the core of the Lyα line and most of the COS spectra show geocoronal airglow of O I at 1310Å. In at least one case, CD-68 2365 in Figure 9, the main-sequence star appears to contribute a noticeable flux towards the red end of the spectrum.

We fitted TLUSTY/SYNSPEC (Hubeny & Lanz 1995) white dwarf model spectra to each of our *HST* observations. With the UV data alone it is not possible to simultaneously solve for the surface gravity, temperature and distance of the white dwarf. Therefore, we fix the mass of the white dwarf at 0.6M$_\odot$ (close to the mean observed value for DA white dwarfs, Liebert et al. 2005; Falcon et al. 2010) and fitted the spectrum to get an estimate of the temperature and distance

for the white dwarf. The best fit models are overplotted in red in Figure 9 and Figure 10 and detailed in Table 2. Note that in the case of LAMOST J1528+4305, where the nature and hence radius of the compact star are unknown, we were unable to determine a reliable distance estimate. We also estimated the distance to the corresponding main-sequence stars in these systems by fitting their spectral energy distributions (SEDs) using the virtual observatory SED analyzer (VOSA; Bayo et al. 2008). We used archival optical data from the TYCHO and NOMAD catalogues and infrared data from the 2MASS and WISE databases. We fitted the SED with BTSettl models (Allard et al. 2012) and kept the physical parameters of the stars (effective temperature, surface gravity and metallicity) fixed at the values from the RAVE and LAMOST databases and scaled the models to best fit the SED, then used the resulting scale factor to determine the distance to the star. The results are listed in Table 2.

In Figure 11 we plot the UV to infrared SEDs of all eight systems observed with *HST* and the best fit white dwarf and main-sequence star models. We do not show the RAVE spectra, since they cover a very small wavelength range (near the Ca II infrared triplet), or the LAMOST spectra, since the flux calibration of LAMOST spectra is relative (Song et al. 2012). We found that in all but one case the distance derived for the white dwarf and main-sequence star in reasonable agreement and therefore the stars are likely in a
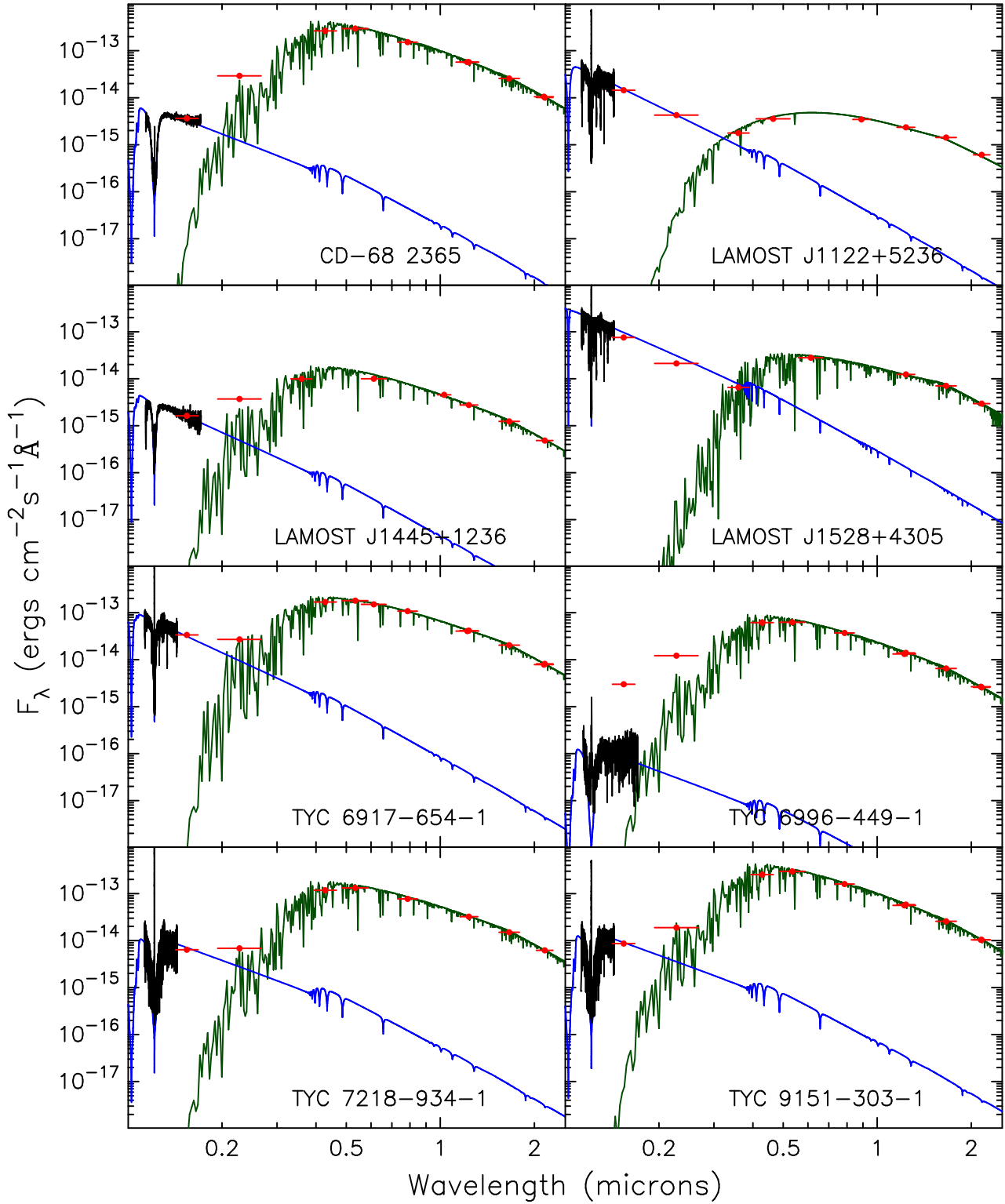
Figure 11. Spectral energy distributions for 8 UV-excess objects observed with *HST*. Photometric measurements are shown in red (errors smaller than the symbol size) and are taken from GALEX (UV), TYCHO and NOMAD (optical) and 2MASS (near-infrared). The *HST* spectra are shown in black. We also plot the best fit model spectra for the white dwarfs (blue lines) and main-sequence stars (green lines). For TYC 6996-449-1 there is a substantial difference between the *HST* flux and GALEX UV measurements. We believe that this is due to the white dwarf and main-sequence star being a spatially resolved binary (or the white dwarf is a background source) separated by a few tenths of an arcsecond. Since the *HST* acquisition for STIS observations is done in the optical the slit may not have been properly centred on the white dwarf (but rather on the main-sequence star) resulting in slit losses.

Table 2. Distance and physical parameter estimates to the white dwarfs (assuming $\log g = 8.0$) and main-sequence stars in the systems observed with *HST*. Typical uncertainties in the white dwarf temperatures are ±500K. The main-sequence star parameters are taken from the RAVE/LAMOST pipelines. A reliable estimate of the distance to the hot component in LAMOST J1528+4305 is not currently possible as the nature of the star (and hence its radius) is unknown.

Target	White dwarf T_{eff} (K)	White dwarf distance (pc)	MS star T_{eff} (K)	MS star $\log g$	MS star $\log Z$	MS star distance (pc)
CD-68 2365	17,500	271	6159 ± 66	3.91 ± 0.13	0.00 ± 0.10	235 ± 20
LAMOST J1122+5236	26,000	430	4437 ± 86	3.95 ± 0.34	-0.71 ± 0.39	505 ± 60
LAMOST J1445+1236	24,000	726	6225 ± 159	4.20 ± 0.46	-0.61 ± 0.40	945 ± 100
LAMOST J1528+4305	24,000	-	4734 ± 47	2.99 ± 0.45	-0.09 ± 0.20	480 ± 55
TYC 6917-654-1	25,000	170	6503 ± 127	4.01 ± 0.21	-0.25 ± 0.13	190 ± 20
TYC 6996-449-1	16,500	1400	5937 ± 95	3.96 ± 0.15	-0.24 ± 0.10	425 ± 40
TYC 7218-934-1	16,500	165	5746 ± 95	3.97 ± 0.15	-0.01 ± 0.10	190 ± 15
TYC 9151-303-1	16,500	151	6161 ± 95	4.63 ± 0.18	0.13 ± 0.11	205 ± 25

physically associated binary, some of which may be PCEBs, which we are aiming to identify in this sample (although additional data are required to confirm this). However, we note that the distance estimates to both stars are subject to systemic uncertainties. For determining the distances to the white dwarfs, we fixed their masses at $0.6M_\odot$, however, if their actual masses are higher (lower) then their radii will be smaller (larger) and hence they will be closer (further) than our estimates. Likewise, the uncertainties on the physical parameters of the main-sequence stars lead to a relatively large spread of possible distances. More accurate and precise distances to the main-sequence stars will soon be available once the results of the *Gaia* mission are published. Only in one system, TYC 6996-449-1, is there is a clear discrepancy between the distance estimates of the two stars, where the implied distance to the white dwarf is more than three times that of the main-sequence star's. Forcing this white dwarf to the same distance as the main-sequence star would require it to have a mass in excess of the Chandrasekhar mass. However, inspection of Figure 11 reveals that the flux of the *HST* spectrum for this object falls substantially below its measured GALEX magnitudes. We believe that this is due to slit losses during the *HST* observations, caused by the fact that acquisition for STIS observations are done in the optical, meaning that the slit is centered on the main-sequence star. If there is a small offset between the main-sequence star and white dwarf (i.e. if this system is a spatially resolved binary or chance alignment), then the 0.2″ slit will not be properly centred on the white dwarf component. This renders the white dwarf distance estimate unreliable and also implies that this system is not a PCEB. However, re-scaling the COS spectrum to fit the GALEX measurements reduces the distance to the white dwarf and brings it into agreement with that of the main-sequence star, therefore, this is likely to be a spatially resolved binary. Despite the fact that the optical and GALEX positional information for this target are coincident to within 0.25″, the resolution and precision of the GALEX astrometry means that we cannot exclude a spatial resolution of a few tenths of an arcsecond between the main-sequence component and the white dwarf in any of our systems. This means that, with the current data, we cannot easily distinguish between PCEBs and main-sequence stars with nearby foreground/background white dwarfs or wide binaries.

5 DISCUSSION

5.1 Sources of contamination

Our sample of UV excess FGK stars contains close PCEBs (at least one has been identified already, Parsons et al. 2015), wide binaries (with spatial separations ≲0.25″) and chance alignments between FGK stars and foreground or background UV bright sources (this includes white dwarfs, but also hot subdwarfs and quasars).

Several other types of object that could potentially contaminate our sample. The hot chromospheres of active stars can result in them possessing quite blue UV colours. Additionally, any active star that flared during GALEX observations may make it into our sample. Previous investigations of FGK stars in SDSS determined that the strong chromospheres of some stars was likely the cause of most UV excesses, particularly at later spectral types (Smith et al. 2014). Recall that SDSS FGK stars are generally too distant to detect any white dwarf companions and therefore the sample is dominated by other types of UV-bright sources. Indeed, several stars in our sample are known to be active and are listed as such in the SIMBAD database. However, the vast majority of these are at the cooler end of our sample and hence are K stars.

As well as isolated active main-sequence stars, stars in close binary systems can be spun-up and become active. Therefore, its possible that our sample is contaminated by some active binaries. These are FGK plus M dwarf binaries in which the unseen M dwarf has been spun-up and a flare from this stars, or its strong chromosphere, is detected by GALEX. Since it appears that most, if not all, M dwarfs in close binaries are active (Rebassa-Mansergas et al. 2013), this may be a source of contamination across our entire sample. Indeed, several objects in our sample are listed as binary stars in SIMBAD (either W UMa or RS CVn type variables). However, the fact that none of the systems we observed with *HST* were these types of binaries implies that the contamination is relatively low.

Finally, we note that RR Lyrae stars can have NUV−FUV colours of between ~3−5 (Kinman & Brown 2014), which places them within our cut. Generally, most RR Lyrae stars are too faint to make it into our sample. However, while there were no known RR Lyrae stars in our RAVE sample, there were 3 in our LAMOST sample (since

the LAMOST sample goes ∼2 mag deeper than RAVE), all of which are at the fainter end of the sample (V>12).

Given that all our *HST* observations confirmed the presence of hot, compact companions we conclude that there are few contaminating sources. However, we note that our *HST* observations mainly cover the larger UV excess objects and therefore more detailed observations are required to better quantify this.

5.2   Testing compact binary evolution

This large sample of white dwarf plus FGK star binaries has the potential to address several important questions relating to the evolution of compact binaries and SN Ia formation. An initial step is to use spectroscopic data to identify the PCEBs within the sample and measure their orbital periods, a task that we have begun. High-resolution imaging can also be used to identify the wide binaries and chance alignments.

One of the most interesting results from the handful of known PCEBs with early-type components is that they can have a much larger range of orbital periods after the CE stage (Zorotovic et al. 2014a). While PCEBs containing M dwarfs generally have periods below ∼10 days (Nebot Gómez-Morán et al. 2011), several PCEBs containing early type stars have much longer periods. For example, the white dwarf plus G5 binary KOI-3278 has a period of 88.2 days (Kruse & Agol 2014), while the white dwarf plus A8 binary IK Peg has a period of 21.7 days (Vennes et al. 1998). Conversely, there are still systems with very short periods such as the 12.5 hour white dwarf plus K2 binary V471 Tau (Nelson & Young 1970) or the 12 hour white dwarf plus F8 binary TYC 6760-497-1 (Parsons et al. 2015). This suggests an additional source of energy is required during the CE phase in order to expel the envelope quickly enough to prevent the two stars getting too close (Zorotovic et al. 2010; Rebassa-Mansergas et al. 2012b), although it is not clear what the source of this energy is (Ivanova et al. 2015). This is particularly relevant to the evolution of double white dwarf binaries, since the two stars must emerge from the first CE far enough apart to survive the second CE phase. So far, models of the CE phase have struggled to simultaneously replicate the observed populations of very close white dwarf plus M dwarf binaries and the population of double white dwarf binaries, requiring two different formalisms to create each population (Nelemans et al. 2000; Toonen & Nelemans 2013). Therefore, a large, well-characterised set of PCEBs with FGK components would be an extremely valuable population for formulating a more complete description of the CE phase itself, since it contains systems that emerged from the CE phase with both very short and long orbital periods.

This is also a particularly important subject for determining the progenitors of SN Ia. Constraining the orbital period distribution of white dwarfs with FGK companions (which will require additional spectroscopic observations) will allow us to determine the fraction of systems following the single and double degenerate formation channels. Moreover, our project has already uncovered one system that will undergo a phase of thermal timescale mass-transfer in the future (Parsons et al. 2015) and hence, in this case, the white dwarf will grow in mass. Given that it may be possible for sub-Chandrasekhar mass white dwarfs to explode as SN Ia

via the double-detonation model it may even be that our sample contains some genuine SN Ia progenitors.

6   CONCLUSIONS

We have presented a large population of 934 bright main-sequence F, G and K type stars with UV excess colours that are likely the result of nearby white dwarf companions. *HST* spectra of nine of these objects has confirmed that these are white dwarf plus main-sequence star binaries (in one case the companion is likely a hot subdwarf star or pre-helium white dwarf) and there appears to be very little contamination, at least among the larger UV excess objects. This previously undetected group of objects has the potential to address a number of key questions relating to binary star evolution and improve our understanding of the common-envelope stage. Moreover, it will also constrain the ratio of binaries that undergo a single common-envelope event to those that will undergo two, with clear implications for the study of type Ia supernovae.

REFERENCES

Allard F., Homeier D., Freytag B., 2012, Royal Society of London Philosophical Transactions Series A, 370, 2765

Althaus L. G., Benvenuto O. G., 1997, ApJ, 477, 313

Barstow M. A., Holberg J. B., Koester D., 1994, MNRAS, 270, 516

Bayo A., Rodrigo C., Barrado Y Navascués D., Solano E., Gutiérrez R., Morales-Calderón M., Allard F., 2008, A&A, 492, 277

Berghöfer T. W., Vennes S., Dupuis J., 2000, ApJ, 538, 854

Bilir S., Karaali S., Ak S., Coşkunoğlu K. B., Yaz E., Cabrera-Lavers A., 2009, MNRAS, 396, 1589

Branch D., Livio M., Yungelson L. R., Boffi F. R., Baron E., 1995, PASP, 107, 1019

Burleigh M. R., Barstow M. A., 1998, MNRAS, 295, L15

Burleigh M. R., Barstow M. A., 1999, A&A, 341, 795

Burleigh M. R., Barstow M. A., Fleming T. A., 1997, MNRAS, 287, 381

Burleigh M. R., Barstow M. A., Holberg J. B., 1998, MNRAS, 300, 511

Carlin J. L., et al., 2012, Research in Astronomy and Astrophysics, 12, 755

Chonis T. S., Gaskell C. M., 2008, AJ, 135, 264

Christian D. J., Vennes S., Thorstensen J. R., Mathioudakis M., 1996, AJ, 112, 258

Claeys J. S. W., Pols O. R., Izzard R. G., Vink J., Verbunt F. W. M., 2014, A&A, 563, A83

Cui X.-Q., et al., 2012, Research in Astronomy and Astrophysics, 12, 1197

Deng L.-C., et al., 2012, Research in Astronomy and Astrophysics, 12, 735

Falcon R. E., Winget D. E., Montgomery M. H., Williams K. A., 2010, ApJ, 712, 585

Fink M., Hillebrandt W., Röpke F. K., 2007, A&A, 476, 1133

Fontaine G., Brassard P., Bergeron P., 2001, PASP, 113, 409

Hillebrandt W., Niemeyer J. C., 2000, ARA&A, 38, 191

Holberg J. B., Bergeron P., 2006, AJ, 132, 1221

Holberg J. B., Oswalt T. D., Sion E. M., McCook G. P., 2016, preprint, (arXiv:1606.01236)

Hubeny I., Lanz T., 1995, ApJ, 439, 875

Hurley J. R., Tout C. A., Pols O. R., 2002, MNRAS, 329, 897

Husser T.-O., Wende-von Berg S., Dreizler S., Homeier D., Reiners A., Barman T., Hauschildt P. H., 2013, A&A, 553, A6

Iben Jr. I., 1982, ApJ, 259, 244

Iben Jr. I., Tutukov A. V., 1984, ApJS, 54, 335

Ivanova N., Justham S., Podsiadlowski P., 2015, MNRAS, 447, 2181

Kahabka P., van den Heuvel E. P. J., 1997, ARA&A, 35, 69

Kinman T. D., Brown W. R., 2014, AJ, 148, 121

Koester D., 2010, Mem. Soc. Astron. Italiana, 81, 921

Kordopatis G., et al., 2013, AJ, 146, 134

Kromer M., Sim S. A., Fink M., Röpke F. K., Seitenzahl I. R., Hillebrandt W., 2010, ApJ, 719, 1067

Kruse E., Agol E., 2014, Science, 344, 275

Landsman W., Simon T., Bergeron P., 1993, PASP, 105, 841

Landsman W., Simon T., Bergeron P., 1996, PASP, 108, 250

Li L., Zhang F., Han Q., Kong X., Gong X., 2014, MNRAS, 445, 1331

Liebert J., Bergeron P., Holberg J. B., 2005, ApJS, 156, 47

Luo A.-L., et al., 2012, Research in Astronomy and Astrophysics, 12, 1243

Luo A.-L., et al., 2015, Research in Astronomy and Astrophysics, 15, 1095

Martin D. C., et al., 2005, ApJ, 619, L1

Maxted P. F. L., Gänsicke B. T., Burleigh M. R., Southworth J., Marsh T. R., Napiwotzki R., Nelemans G., Wood P. L., 2009, MNRAS, 400, 2012

Maxted P. F. L., et al., 2014, MNRAS, 437, 1681

Mestel L., 1952, MNRAS, 112, 583

Napiwotzki R., et al., 2001, Astronomische Nachrichten, 322, 411

Nebot Gómez-Morán A., et al., 2011, A&A, 536, A43

Nelemans G., Tout C. A., 2005, MNRAS, 356, 753

Nelemans G., Verbunt F., Yungelson L. R., Portegies Zwart S. F., 2000, A&A, 360, 1011

Nelemans G., Yungelson L. R., Portegies Zwart S. F., Verbunt F., 2001, A&A, 365, 491

Nelson B., Young A., 1970, PASP, 82, 699

Nomoto K., Kondo Y., 1991, ApJ, 367, L19

Paczynski B., 1976, in Eggleton P., Mitton S., Whelan J., eds, IAU Symposium Vol. 73, Structure and Evolution of Close Binary Systems. p. 75

Parsons S. G., et al., 2012, MNRAS, 426, 1950

Parsons S. G., et al., 2015, MNRAS, 452, 1754

Raymond S. N., et al., 2003, AJ, 125, 2621

Rebassa-Mansergas A., Gänsicke B. T., Rodríguez-Gil P., Schreiber M. R., Koester D., 2007, MNRAS, 382, 1377

Rebassa-Mansergas A., Nebot Gómez-Morán A., Schreiber M. R., Gänsicke B. T., Schwope A., Gallardo J., Koester D., 2012a, MNRAS, 419, 806

Rebassa-Mansergas A., et al., 2012b, MNRAS, 423, 320

Rebassa-Mansergas A., Schreiber M. R., Gänsicke B. T., 2013, MNRAS, 429, 3570

Rebassa-Mansergas A., Ren J. J., Parsons S. G., Gänsicke B. T., Schreiber M. R., García-Berro E., Liu X.-W., Koester D., 2016, MNRAS,

Ruiter A. J., Belczynski K., Fryer C., 2009, ApJ, 699, 2026

Shara M. M., Prialnik D., Shaviv G., 1977, A&A, 61, 363

Silvestri N. M., et al., 2006, AJ, 131, 1674

Sim S. A., Röpke F. K., Hillebrandt W., Kromer M., Pakmor R., Fink M., Ruiter A. J., Seitenzahl I. R., 2010, ApJ, 714, L52

Simon T., Fekel Jr. F. C., Gibson D. M., 1985, ApJ, 295, 153

Smith M. A., Bianchi L., Shiao B., 2014, AJ, 147, 159

Song Y.-H., et al., 2012, Research in Astronomy and Astrophysics, 12, 453

Toonen S., Nelemans G., 2013, A&A, 557, A87

Toonen S., Nelemans G., Portegies Zwart S., 2012, A&A, 546, A70

Torres G., Andersen J., Giménez A., 2010, A&ARv, 18, 67

Tutukov A. V., Yungelson L. R., 1979, Acta Astron., 29, 665

Vennes S., Mathioudakis M., Doyle J. G., Thorstensen J. R., Byrne P. B., 1995, A&A, 299, L29

Vennes S., Christian D. J., Mathioudakis M., Doyle J. G., 1997, A&A, 318, L9

Vennes S., Christian D. J., Thorstensen J. R., 1998, ApJ, 502, 763

Wang B., Han Z., 2012, New Astron. Rev., 56, 122

Webbink R. F., 1984, ApJ, 277, 355

Willems B., Kolb U., 2004, A&A, 419, 1057

Wu Y., Du B., Luo A., Zhao Y., Yuan H., 2014, in Heavens A., Starck J.-L., Krone-Martins A., eds, IAU Symposium Vol. 306, IAU Symposium. pp 340–342 (arXiv:1407.1980), doi:10.1017/S1743921314010825

Xiang M. S., et al., 2015, MNRAS, 448, 90

Yoon S.-C., Podsiadlowski P., Rosswog S., 2007, MNRAS, 380, 933

Yuan H.-B., et al., 2015, MNRAS, 448, 855

Yungelson L. R., Livio M., Tutukov A. V., Saffer R. A., 1994, ApJ, 420, 336

Zhao G., Zhao Y.-H., Chu Y.-Q., Jing Y.-P., Deng L.-C., 2012, Research in Astronomy and Astrophysics, 12, 723

Zorotovic M., Schreiber M. R., Gänsicke B. T., Nebot Gómez-Morán A., 2010, A&A, 520, A86

Zorotovic M., Schreiber M. R., Parsons S. G., 2014a, A&A, 568, L9

Zorotovic M., Schreiber M. R., García-Berro E., Camacho J., Torres S., Rebassa-Mansergas A., Gänsicke B. T., 2014b, A&A, 568, A68

Zorotovic M., et al., 2016, MNRAS, 457, 3867

van den Heuvel E. P. J., Bhattacharya D., Nomoto K., Rappaport S. A., 1992, A&A, 262, 97

APPENDIX A: RAVE UV-EXCESS TARGETS

APPENDIX B: LAMOST UV-EXCESS TARGETS

This paper has been typeset from a TeX/LaTeX file prepared by the author.

Table A1. Main-sequence stars from the RAVE survey with UV-excesses. The full table is available online.

SIMBAD Name	RA	Dec	FUV	NUV	V	T_{eff} (K)	$\log g$	$\log Z$
UCAC3 131-28	00:00:44.521	-24:41:16.62	22.246	19.969	11.960	4482	4.53	-0.06
2MASS J00005502-5738534	00:00:55.031	-57:38:53.23	22.426	19.399	12.199	4719	4.35	0.29
TYC 6992-827-1	00:01:13.398	-33:27:06.73	18.014	16.944	11.053	5091	3.62	-0.16
UCAC2 17856213	00:03:08.614	-32:49:52.76	20.843	18.390	12.560	5106	3.60	-0.21
TYC 1-890-1	00:04:21.129	+01:09:14.46	19.248	18.563	11.141	5021	3.71	-0.09
BD-13 6521	00:07:09.421	-12:22:21.98	14.877	14.205	10.962	5743	4.77	-1.07
TYC 5263-340-1	00:07:34.891	-11:46:27.41	21.791	18.300	11.238	4646	4.75	0.60
CD-44 16	00:08:44.585	-43:42:24.73	20.064	16.185	10.519	5884	4.26	0.08
TYC 8467-109-1	00:09:48.371	-56:45:01.94	20.820	17.120	11.377	5287	4.68	-0.04
CD-26 60	00:14:12.099	-26:05:50.77	15.432	13.741	10.230	6456	4.06	-0.54
TYC 9134-1979-1	00:15:12.269	-68:50:58.49	21.805	19.077	8.760	5250	5.00	-4.00
TYC 6419-603-1	00:15:14.881	-28:47:54.68	22.110	18.788	11.723	4574	4.28	0.72
CD-30 57	00:15:19.606	-29:46:15.89	17.703	16.183	11.523	5642	4.97	-0.27
LTT 128	00:16:24.466	-46:43:11.41	20.114	18.999	11.084	4348	4.86	-0.04
TYC 4670-766-1	00:17:32.176	-07:21:13.52	18.686	15.975	10.391	5308	4.56	-0.16
UCAC2 10774801	00:19:01.431	-48:53:36.44	21.615	18.729	12.190	4294	3.67	0.99
TYC 6996-449-1	00:19:07.381	-37:12:35.20	17.961	15.593	11.964	6162	4.04	-0.56
2MASS J00212706-1101097	00:21:27.068	-11:01:09.70	21.164	17.889	12.130	5246	4.34	-0.50
2MASS J00214219-4140026	00:21:42.197	-41:40:02.60	22.396	20.485	13.460	4000	4.78	-0.50
2MASS J00224832-6047096	00:22:48.324	-60:47:09.68	21.500	19.142	12.150	4673	4.92	0.06
...	...	...	...	...	...	...	...	...

Table B1. Main-sequence stars from the LAMOST survey with UV-excesses. The full table is available online.

LAMOST Name	RA	Dec	FUV	NUV	g or r(*)	T_{eff} (K)	$\log g$	$\log Z$
J0006+0247	00:06:40.63	+02:47:04.9	20.637	18.941	15.48	6433	4.26	-0.27
J0009+0420	00:09:48.87	+04:20:43.5	18.869	18.653	14.90	5801	4.01	-0.50
J0010+3445	00:10:38.07	+34:45:34.3	19.435	18.633	13.70*	5881	4.26	-0.30
J0011+3416	00:11:43.58	+34:16:16.7	20.331	18.741	12.97*	5734	4.46	0.05
J0012+3424	00:12:33.67	+34:24:31.8	15.865	14.850	10.90*	6535	4.15	-0.15
J0013+3135	00:13:38.16	+31:35:12.3	18.698	17.501	11.32*	5749	4.25	0.55
J0016+3002	00:16:41.20	+30:02:38.4	19.261	15.496	9.83*	5181	2.70	-0.23
J0017+0521	00:17:42.15	+05:21:10.0	18.985	19.211	18.41	4744	2.54	-1.20
J0021+3342	00:21:22.99	+33:42:37.1	19.637	17.064	10.49*	4755	3.33	-0.37
J0022+3322	00:22:39.48	+33:22:16.7	19.754	19.199	13.25*	5188	4.52	0.32
J0034+3951	00:34:16.74	+39:51:05.8	20.066	19.513	15.30	4361	4.61	-0.30
J0040+4057	00:40:07.81	+40:57:56.7	22.396	19.676	15.62	6002	3.98	-0.43
J0044+4138	00:44:33.80	+41:38:28.5	21.751	20.241	16.75	5887	4.04	-0.56
J0047+0319	00:47:05.92	+03:19:54.8	17.338	16.414	15.96	5114	3.38	-0.96
J0047+3944	00:47:38.86	+39:44:11.6	19.480	17.767	14.87	6715	4.53	-0.45
J0048+2706	00:48:04.18	+27:06:57.6	18.385	16.414	12.48	6370	4.15	-0.06
J0049+3919	00:49:27.53	+39:19:18.9	20.679	19.128	16.04	6848	4.10	-0.49
J0051+3925	00:51:03.61	+39:25:35.0	22.054	21.498	15.73	4770	2.65	-0.68
J0057+3625	00:57:46.23	+36:25:07.0	20.039	18.819	15.34	6010	4.25	-0.26
J0058+0235	00:58:23.64	+02:35:56.7	18.157	14.235	11.64	5535	4.06	-0.45
...	...	...	...	...	...	...	...	...